International Journal of Green Energy

ISSN: 1543-5075 (Print) 1543-5083 (Online) Journal homepage: http://www.tandfonline.com/loi/ljge20

Thermally Chargeable Supercapacitor Based on Nickel-Coated Nanoporous Carbon

Hyuck Lim, Yang Shi & Yu Qiao

To cite this article: Hyuck Lim, Yang Shi & Yu Qiao (2017): Thermally Chargeable Supercapacitor Based on Nickel-Coated Nanoporous Carbon, International Journal of Green Energy, DOI: 10.1080/15435075.2017.1313737

To link to this article: http://dx.doi.org/10.1080/15435075.2017.1313737

Accepted author version posted online: 12 Apr 2017.

Thermally Chargeable Supercapacitor Based on Nickel-Coated Nanoporous Carbon

Hyuck Lim,[1] Yang Shi,[1] Yu Qiao[1,2,*]

[1] *Program of Materials Science and Engineering, University of California, San Diego, La Jolla, CA, USA*

.[2] *Department of Structural Engineering, University of California, San Diego, La Jolla, CA, USA.*

[*] *Corresponding author. Program of Materials Science and Engineering, University of California, San Diego, 92093, La Jolla, CA, USA. Email: yqiao@ucsd.edu. Phone: +1-858-534-3388*

Abstract

Nanoporous carbon is coated by pure nickel via an electroless plating method. The nanoporous carbon provides a high-surface-area substrate, leading to a large capacitance; the nickel surface layer is of a high work function, resulting in a thermally sensitive electrode potential. Such a system is ideal for thermally chargeable supercapacitor (TCS) system, which converts low-grade heat (LGH) to electrical energy. The specific energy per thermal cycle per gram of electrode mass is ~1.8 mJ, with a temperature difference of 50 ^{o}C.

Keywords: Capacitive; Energy conversion; Low-grade heat; Nanoporous carbon; Coating

Introduction

Harvesting low-grade heat (LGH), i.e. thermal energy from heat sources below 300-400 ^{o}C, is an attractive yet technologically challenging research topic. On the one hand, LGH is ubiquitous and ample. In the U.S. alone, hundreds of Giga Watts of LGH is wasted in cooling systems in fossil fuel and nuclear power plants [1]. Other important LGH sources include geothermal energy, ocean thermal energy, waste heat in vehicle engines, etc. [2]. If they can be harvested and utilized, the overall energy efficiency can be largely enhanced. On the other hand, due to the relatively low temperature, less thermal energy can be provided by a LGH source; moreover, the efficiency of any thermal to electrical energy conversion (TEEC) process cannot exceed the Carnot cycle limit, yet the limit for LGH is inherently low [3]; even more critically, the TEEC efficiency of conventional techniques, either direct approaches based on the Seebeck effect of thermoelectrics [4] or indirect approaches using organic Rankine cycle (ORC) machines [5], tends to be low in the LGH temperature range [6]. Consequently, only a small portion of the already low-energy-density LGH can be converted to electrical energy, which does not cover the relatively high materials cost of thermoelectrics or maintenance/operational costs of ORC machines [7]. New mechanisms must be discovered to compete with the low cost of grid power; otherwise LGH utilization may not be economically feasible.

In view of the above consideration, we developed a direct TEEC technique fundamentally different from thermoelectrics: thermally chargeable supercapacitors (TCS), specifically for LGH sources [8]. Supercapacitor is an important energy storage device, having a high power density and a long cycle life, often up to millions of cycles [9]. Its performance is usually thermally dependent: As temperature changes, due to the variation of electrode potential,

the output voltage may be different. While this thermal effect is detrimental in many cases, its inverse process enables the TCS technique. In a TCS, two half supercapacitors (HSC) are placed at different temperatures and connected through a salt bridge, as depicted in Fig.1. Each HSC consists of a nanoporous electrode immersed in an electrolyte solution. At the high-temperature side, the electrode potential is different from at the low-temperature side; thus, as the two electrodes form a circuit via an external resistor, R_0, a current is generated. When a new equilibrium is reached, the current would vanish and the TCS system must be reactivated, e.g. by switching the positions of the two HSC between the high-temperature and low-temperature sides. Advantages of TCS include the high output voltage, the high effective electrical conductivity, and the low effective thermal conductivity, which lead to a large output voltage and a high TEEC efficiency.

The TCS performance is determined by two key factors: thermal sensitivity of electrode potential, $\mathrm{d}V/\mathrm{d}T$, and surface charge, Q. For a given temperature difference, ΔT, the harvested electrical energy may be assessed through $U \propto Q\cdot(\mathrm{d}V/\mathrm{d}T)\cdot\Delta T$. Our experimental data have shown that a smaller cation size [10], a large anion size [11], and a high dielectric constant of solvent [12] are beneficial to develop a highly thermally sensitive TCS system; i.e. to achieve a large value of $|\mathrm{d}V/\mathrm{d}T|$; while the ion concentration effect is secondary is a broad range [13]. A more recent result suggests that the electrode material is also a vital factor [14]: when the work function of the electrode material is relatively low, e.g. indium (In), the variation of electrode potential is quite random over a large temperature range; when the work function is relatively high, e.g. nickel (Ni) or platinum (Pt), the electrode potential rises rapidly with temperature, resulting in a large output voltage with a small temperature difference. However, conventional solid Ni and Pt electrodes have small specific surface areas, A, and therefore, their surface

charges, *Q*, are low. While nanostructured metallic materials have been developed via a variety of methods [e.g. 15], the processing cost is typically high, which is contradictory to the fundamental goal of the TCS development, to compete against the grid power cost. A promising approach to circumvent this problem is to coat a high-work-function metal, e.g. Ni, on a large-surface-area substrate, e.g. a nanoporous carbon, which will be the focus of the current study.

Experimental

Electroless deposition technique was employed to coat Ni on Cabot BP2000 nanoporous carbon (NC), following the work of Arai et al. [15]. By using a Micrometritics TriStar-3000 Gas Absorption Analyzer, a Brunauer-Emmett-Teller (BET) analysis was performed and the specific surface area of the NC was measured as 1810 m^2/g. The nanopore size ranged from less than 1 nm to 100 nm, exhibiting a bimodal distribution with the peaks at 3 nm and 50 nm. The NC powders were rinsed by distilled water and then vigorously stirred and refluxed in an acidic solution containing 1 part of nitric acid (HNO_3) and 3 parts of sulfuric acid (H_2SO_4) for 4 h. The acid washed NC was immersed in an aqueous solution of 0.05 mol/L tin chloride dihydrate ($SnCl_2 \cdot 2H_2O$) and 0.1 mol/L chlorine acid (HCl) for 10 min at 25°C, and ultrasonically agitated. After filtration and thorough rinsing, the surface activated NC was immersed in an aqueous solution of 5.6×10^{-4} mol/L palladium chloride ($PdCl_2$) and 0.12 mol/L chlorine acid (HCl) for 30 min at 25°C, and ultrasonically agitated to form palladium catalytic nuclei on carbon surfaces. After filtration and thorough rinsing, the NC powders were placed in an electroless nickel plating bath, which contained 0.05 M nickel chloride hydrate ($NiCl_2 \cdot 6H_2O$), 0.5 M gluconic acid ($C_6H_{12}O_7$), 0.4 M hydrazine monohydrate ($N_2H_4 \cdot H_2O$), and 0.5 M boric acid (H_3BO_3). The pH

value was adjusted to 12. Electroless plating was performed at 80 °C with stirrer agitation for 24 h. After filtration and through rinsing, the nickel-coated nanoporous carbon (NiNC) was dried in air, and thermally reduced in a 5% hydrogen forming gas environment at 500 °C for 1 h by using a tube furnace.

About 20 mg of NiNC was compacted on a platinum (Pt) foil under a high pressure around 400 MPa in a stainless steel cylindrical mold by using a type 5582 Instron machine, to produce an electrode disk. Figure 2 shows a SEM image of the close-paced NiNC grains in an electrode. The Pt foil was nearly 1 cm^2 large and served as charge collector. To form a HSC cell, a NiNC electrode was immersed in 1 M formamide (FA) solution of anhydrous sodium acetate ($NaC_2H_3O_2$) in a polypropylene (PP) container.

A through-hole channel was created between two identical HSC cells and filled by the electrolyte solution, which became a salt bridge. The two electrodes were connected through a switch and a 200 Ω resistor, R_0 (Fig.1). The salt bridge was 5 mm in diameter and 30 mm in length. By using a Corning PC-220 hot plate, one of the HSC cell was heated at the rate of 3 ^oC/min. The temperature range was from room temperature (25 ^oC) to about 70 ^oC. The other HSC cell was kept at room temperature in a cold water jacket throughout the testing procedure. The temperatures of the cells were monitored by type-K thermocouples via a National Instrument HH-20A Reader. A reference system was assembled with a similar structure, except that the NiNC electrodes in HSC cells were replaced by pure Ni foils.

As the temperature difference between the two HSC cells, ΔT, increased, the switch was turned off. The open-circuit output voltage between the two electrodes, V, was measured by a National Instrument SCB68 data acquisition (DAQ) system. Figure 3 shows typical V-ΔT curves of the reference Ni electrode as well as the NiNC electrode. When the maximum ΔT was reached,

the switch was turned on, and the close-circuit voltage on R_0 was measured, as demonstrated in Fig.4. Due to the small capacitance of Ni electrode, no current could be detected in the reference system, and therefore, only the curve for the NiNC TCS is shown.

Results and Discussion

The electroless coating of Ni on NC is promoted by the acid washing, which activates more surface hydroxyl and carboxylic functional groups. The coating bath contains 12 ml of gluconic acid and 5 ml of hydrazine per 100 ml of solution, as complexing and reducing agents for nickel ions, respectively. As a result, a uniform Ni layer is created on the surfaces of NC grains [15]. Figure 2 shows that the characteristic length scale of the NC phase is around 100 nm. Associated with the SEM imaging, an energy dispersive x-ray (EDX) spectroscopy analysis is conducted. The main components of NiNC are carbon (C), oxygen (O), nickel (Ni), and tin (Sn), with the weight percentages of 67%, 11.45%, 19.4%, and 2.15%, respectively; and the atomic percentages of 84%, 10.77%, 5%, and 0.27%, respectively. Oxygen and tin may come from the electroless plating process as well as the residual hydroxyl and carboxylic groups. The 5 at% Ni content suggests that the Ni coating thickness is nearly 10% of the ligament length of NC, i.e. a few nm, which looks plausible.

The nickel surface layer has a relatively high work function (WF) of 5.2 eV; WF of the pristine carbon surfaces and many other metallic electrodes are much lower [16]. According to the Jellium model [17], as temperature (T) changes, the electrode potential (V) varies with the density of the positive ions, n^+; and the n^+ is closely correlated with WF. It is equivalent to adding a third capacitive component that takes account for the solid phase effects into the Gouy-

Chapman model of the electrode-electrolyte interface, in addition to the capacitive components associated with the Helmholtz layer and the diffusion layer. Consequently, the electrode potential of an electrode of a higher WF tends to be more thermally sensitive; that is, it has a higher value of dV/dT.

When the working electrodes in TCS are Ni foils, in a previous experiment we showed that, due to the large WF value, when the electrolyte is a 1 M formamide solution of lithium chloride (LiCl), the thermal sensitivity of electrode potential was as high as 4 mV/^{o}C [14]; that is, with a relatively small temperature difference of 50 ^{o}C, the output voltage reached 0.2 V. However, the threshold voltage of electrochemical reaction of this system is quite low [18]. To keep the thermal processes in the electro-physical domain, in the current study the electrolyte is chosen as 1 M sodium acetate. It shows negligible galvanic effects in the temperature and potential ranges under investigation, which should be related to the relatively less polar structures of sodium and acetate ions, compared with lithium and chlorine ions. For instance, it is easier to form an adsorbed chlorine ion surface layer than acetate ion.

As temperature difference between the two HSC cells rises, as shown by Fig.3, the open-circuit output voltage increases monotonously. When the electrode is reference Ni foil, with a ΔT of 45 ^{o}C, the output voltage, V, reaches 80 mV. For self-comparison purpose, a nominal thermal sensitivity of electrode potential, dV/dT, is defined as the maximum voltage divided by the maximum temperature change. For the reference TCS, dV/dT is around 1.8 mV/^{o}C. Not that the V-ΔT relation is nonlinear. When ΔT is below 20 ^{o}C, the output voltage is quite small, only less than 20 mV; when ΔT increase from 20 to 40 ^{o}C, the output voltage rapidly rises and reaches a steady state. The effective dV/dT in the relatively linear high-ΔT section is ~2.5 mV/^{o}C.

When the electrodes are NiNC, the main characteristics of the V-ΔT relation are similar with that of the reference system, expect dV/dT is slightly larger, around 2.1 mV/^{o}C. The similarity suggests that the Ni coating on the NC substrate is nearly complete and uniform. As the electrode-electrolyte interface is governed by the Ni surface layer, the NC phase provides a conductive support and its influence on electrode potential is negligible. The slight difference may be caused by the relatively small amount of Sn impurity on the NiNC electrodes, which changes the effective WF. It can also be attributed to the nanoporous configuration of NiNC: Because the solvated ions at the electrode-electrolyte interface in a nanopore are confined by the nanopore wall from all the directions, the effective surface ion density tends to be higher than at a large, flat Ni foil surface [18-20].

While the reference Ni electrode offers a similar open-circuit output voltage, due to its small surface area, the total ionic charges that accumulate in the surface double layer are trivial. Thus, as the switch in the TCS system is turn on and the two HSC cells are connected by the finite resister, R_0, a new equilibrium would be established instantaneously; the voltage across the resistor would drop to zero before the DAQ system can detect it. For the NiNC system, thanks to the large specific surface area, the capacitance is much larger. Hence, a transient current can be measured from the resistor for a long time, up to tens of hours, before the voltage fully vanishes (Fig.4). For a single energy harvesting cycle with a temperature difference of 50 ^{o}C, the specific output electrical energy is calculated as $U = \int(V^2/R_0)\mathrm{d}t$ = 1.8 mJ per gram of NiNC electrode mass, where t represents time. For a small scale TCS, thermal equilibrium may be achieved in 10-20 sec, and therefore, the effective power is around 0.1 mW/g, much higher than that of conventional thermoelectrics in the same LGH temperature range.

Concluding Remarks

To summarize, nickel-coated nanoporous carbon (NiNC) is employed as electrodes in thermally-chargeable supercapacitors (TCS). The NiNC electrode has a large surface area, thanks to the nanoporous carbon substrate; and a high work function, due to the nickel surface coating. Thus, when it is immersed in an electrolyte solution and temperature varies, a large change in electrode potential is achieved, accompanied by a significant electrical energy generation. With a relatively small temperature difference of 50 ^{o}C, the specific energy is ~1.8 mJ per gram of electrode mass per thermal cycle, and the estimated output power is ~0.1 mW per gram of electrode mass. Such a system may be used to convert low-grade heat (LGH) to electrical energy.

Funding

The experimental research was supported by the National Science Foundation under Grant No. ECCS-1028010. The data analysis was supported by the Advanced Research Projects Agency – Energy under Grant No. DE-AR0000396.

References

1. R. Lasseter and P. Paigi, presented at PESC 04. IEEE 35th Annual, Power Electronics Specialists Conf., 35th Annual IEEE Power Electronics Specialists Conf., 2004
2. D. Tanner, Renew. Energy. **6**, 367 (1995).
3. G. Nolas, J. Sharp and H. Goldsmid, Thermoelectrics: Basics Principles and New Materials Developments (Springer-Verlag, Berlin, 2001), p. 12.
4. M. Dresselhaus, G. Chen, M. Tang, R. Yang, H. Lee, D. Wang, Z. Ren, J. Fleurial and P. Gogna, Mater. Res. Soc. Symp. Proc. **886**, 1 (2006).
5. T. Wang, Y. Zhang, Z. Peng, and G. Shu, Renew. Sustainable Energy Rev. **15**, 2862 (2011).
6. W. Husband and A. Beyene, Int. J. Energy Res. **32**, 1373 (2008).
7. T.C. Hung, T. Y. Shai and S. K. Wang, Energy. **22**, 661 (1997).
8. Y. Qiao, V.K. Punyamurtula, A. Han and H. Lim, J. Power Sources. **183**, 403 (2008).
9. R. Kötz and M. Carlen, Electrochim. Acta. **45**, 2483 (2000).
10. H. Lim, W. Lu and Y. Qiao, Appl. Phys. Lett. **101**, 063902.1 (2012).
11. H. Lim, W. Lu, X. Chen and Y. Qiao, Inter. J. Electrochem. Sci. **7**, 2577 (2012).
12. H. Lim, C. Zhao and Y. Qiao, Phys. Chem. Chem. Phys. **16**, 12728 (2014).

13. H. Lim, W. Lu, X. Chen and Y. Qiao, Nanotech. **24**, 465401.1 (2013).

14. H. Lim, Y. Shi, M. Wang and Y. Qiao, *Appl. Phys. Lett.* **106**, 223901.1 (2015)

15. S. Arai, M. Kobayashi, T. Yamamoto and M. Endo, Electrochem. Solid-State Lett. **13** D94 (2010).

16. D.R. Lide, CRC Handbook of Chemistry and Physics (CRC press, Boca Raton, 2009) 85th ed., p. 12-130

17. W. Schmickler and D. Henderson, Prog. Surf. Sci. **22**, 323 (1986).

18. W. Lu, T. Kim, C. Zhao, X. Chen and Y. Qiao, Appl. Phys. A-Mater. Sci. Proc. **112**, 885 (2013).

19. W. Lu, T. Kim, C. Zhao and Y. Qiao, Inter. J. Mater. Res. **104**, 594 (2013).

20. W. Lu, T. Kim, A. Han and Y. Qiao, Mater. Chem. Phys. **133**, 259 (2012).

Figure 1. Schematic of the thermally-chargeable supercapacitor (TCS).

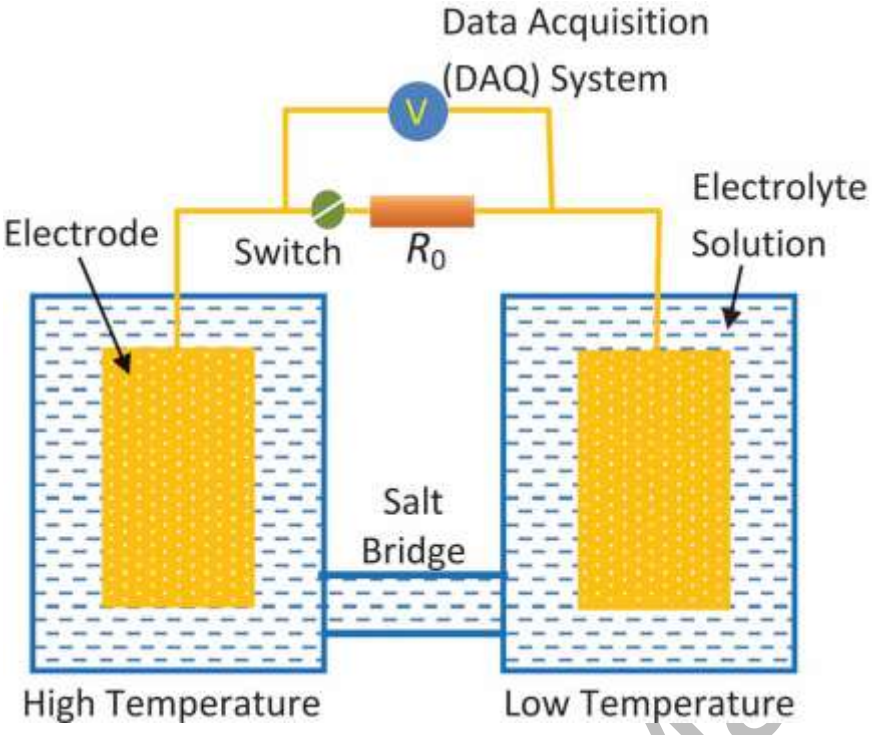

Figure 2. SEM image of a nickel-coated nanoporous carbon (NiNC) electrode.

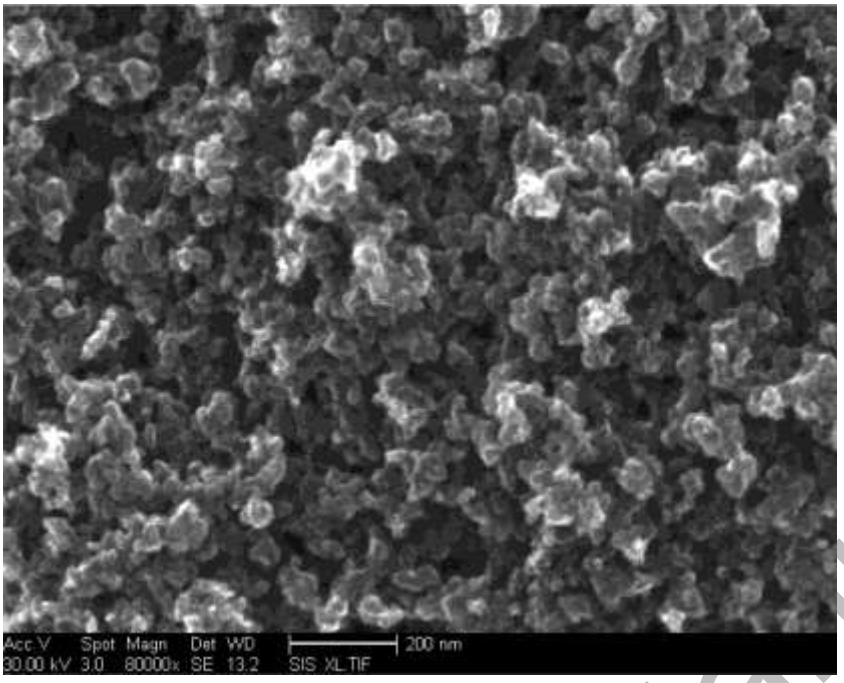

Figure 3. Typical thermal sensitivity curves of reference nickel electrode and nickel-coated nanoporous carbon electrode, in 1 M formamide solution of sodium acetate.

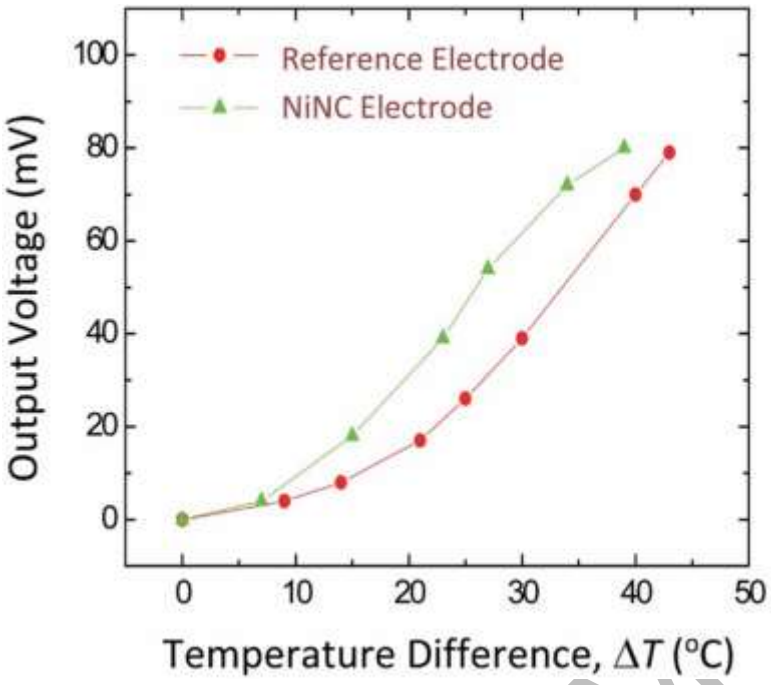

Figure 4. A typical discharge curve of nickel-coated nanoporous carbon system.